BRNO UNIVERSITY OF TECHNOLOGY

VYSOKÉ UČENÍ TECHNICKÉ V BRNĚ

FACULTY OF ELECTRICAL ENGINEERING AND COMMUNICATION

FAKULTA ELEKTROTECHNIKY
A KOMUNIKAČNÍCH TECHNOLOGIÍ

DEPARTMENT OF RADIO ELECTRONICS

ÚSTAV RADIOELEKTRONIKY

AN OPTICAL D/A CONVERTER FOR VLC APPLICATIONS

OPTICKÝ D/A PŘEVODNÍK PRO VLC APLIKACE

SHORT VERSION OF PHD THESIS

ZKRÁCENÁ VERZE DIZERTAČNÍ PRÁCE

AUTHOR
AUTOR PRÁCE

Ing. Aleš Dobesch

SUPERVISOR
ŠKOLITEL

prof. Ing. Otakar Wilfert, CSc.

BRNO 2017

Keywords: LED, VLC, ODAC, channel modeling, photo diode, optical modulation, optical receiver.

Klíčová slova: LED, VLC, ODAC, modelování kánalu, fotodioda, optické modulace, optický přijímač.

Rukopis disertační práce je uložen na:
Ústav Radioelektroniky
Fakulta elektrotechniky a komunikačních technologií
Vysoké učení technické v Brně
Technická 3082/12
616 00 Brno

Contents

INTRODUCTION

In the last few years, general lighting has undoubtedly been one of the most emerging technologies. Light emitting diodes (LEDs) are gradually replacing conventional lighting devices due to their excellent intrinsic characteristics. Among these characteristics, efficacy, relatively long lifetime (the order of 100,000 hours [16]), low cost and enhanced control are perhaps the most relevant aspects which make these devices superior compared to conventional devices such as incandescence or even compact fluorescent lamps. In terms of luminous efficacy, state-of-the-art high power LEDs are now able to exceed 300lm/W for phosphorous coated devices [5]. The immense impact on the lighting industry demonstrates, for instance, the transition to pure LED technology in automotive or in general the lighting industry. A similar trend is obvious in other branches including modern architecture, healthcare, vehicle telematics, security or even agriculture. The accelerated LED production predetermines solid state lighting (SSL) as a future technology for general lighting.

LEDs, organic LEDs (OLEDs) or other LED-based devices in combination with suitable modulation techniques allows to employ them not only for lighting but also for communication purposes. The usage of LEDs as communicating devices was proposed by Nakagawa in 2000 [18]. The technological concept known as visible light communication (VLC) has been associated by the group Visible light communication consortium (VLCC). Afterwards, this communication technology via visible light is better known under the term Light-Fidelity (Li-Fi) coined by prof. Harald Haas [13]. VLC technology, similar in nature to the more mature infra-red (IR) wireless based systems, presents the advantage of exploiting the same device for both lighting and communications means. This way, LEDs are used to convey information, while performing their normal lighting function. The human eye cannot detect fast light fluctuations (more than 200Hz), being sensitive only to average luminous power. Thus, it is possible to modulate the light with fast changing signals.

The connection of lighting and communication seems to be a feasible opportunity for current wireless indoor systems. The most often cited case predisposes VLC as a suitable alternative for Wi-Fi especially in all day illuminated offices. Another significant VLC utilization is relevant in RF restricted areas. As regards to outdoor applications, VLC has a good chance to enhance vehicle telematics, traffic safety and fluency.

The dissertation thesis deals with a VLC system employing a nontraditional transmitter concept based on optical digital to analog conversion (ODAC). Based on a complex numerical model the thesis examines several possible ODAC-based transmitter architectures suitable for VLC applications. The thesis deeply explores and evaluates several VLC system set-ups ready to use advanced modulation techniques in terms of channel modeling. The experimental part evaluates overall performance of two ODAC samples. Finally, the thesis demonstrates ODAC transmitter performance using a real-time VLC system designed on a field programmable gate array (FPGA).

1 OBJECTIVES OF THE THESIS

VLC is a highly perspective area of modern wireless communication. Unlike the conventional transmitter front-end, the ODAC concept is able to cope with LED driving constraints with no need of electrical DAC in the transmitter stage. Therefore, ODAC is an ideal candidate to participate with advanced modulation schemes, for instance OFDM-based modulation tailored for VLC.

The dissertation thesis is focused on analyzing and designing a VLC system using ODAC array as the transmitter front-end. Although the ODAC concept has already been proposed, there exists no study which deeply explores VLC channel modeling. Furthermore, there exists no research dealing with real time VLC systems employing the ODAC concept as the transmitter front-end. The most relevant dissertation objectives can be summarized as follows:

Dissertatition objectives

1. Based on previous findings, the first aim is to create a suitable simulation model for studying multipath optical signal propagation of VLC systems employing the ODAC concept. In further steps, the VLC simulation model will be used to determine a suitable ODAC architecture with respect to transmitter dimensions and transmitter bit resolution.
2. The following objective is to design an ODAC-based VLC system using the previously developed simulation model. In this second objective the overall system performance will be revealed.
3. The third aim is to design an ODAC emitter hardware implementation and evaluate the overall performance of the ODAC sample. The key ODAC emitter parameters as well as a practical demonstration of a real time communication ODAC-based system will be explored.

2 VLC SYSTEM MODELING

This chapter describes in detail the VLC system model able to study the ODAC communication system performance in terms of transmitter architecture, multi-path optical signal propagation and geometrical relations between the transmitter, optical channel and the receiver. The proposed numerical model is based on the modified Barry's method implemented in the MATLAB environment. A suitable ODAC emitter architecture is chosen based on preliminary simulation results. Furthermore, several optical channel scenarios are demonstrated in order to explore the ODAC communication system performance.

2.1 VLC system models

The proposed VLC system model may be split into three fundamental parts, more specifically, into the emitter model, the reflection model and the receiver model. In the following lines, the mathematical definition of the individual models is described.

2.1.1 Emitter model

In VLC the transmitter is formed by a source of radiation which operates in the visible area of the electromagnetic spectrum. As a general rule, in VLC domain the system transmitter always employs LEDs or an array of LEDs as a visible light source. Due to the relatively short switching time the LEDs are ideal for further modulation and high speed data transfers. System transmitting active areas for LoS links as well as for non-LoS links could be ideally modeled with a generalized Lambertian model. More specifically, optical transmitting intensity distribution is a cosine function of angle.

Practical approximation of $I_{\mathrm{Tx}}(\theta)$ can be expressed by the following formula (2.1):

$$I_{\mathrm{Tx}}(\theta) = I_0 \cos^n(\theta), \tag{2.1}$$

where θ is the viewing angle of transmitter, I_0 is radiant intensity normal to the LED source, n characterizes the directivity index of the LED, defined by the *HPA* $\theta_{1/2}$ ($n = 1$ corresponds to a traditional Lambertian source). From the definition $I_{\mathrm{Tx}}(\theta_{1/2})/I_0$ at the half angle is 0.5. Mathematically, n can be then derived from (2.2):

$$\cos^n(\theta_{1/2}) = 0.5, \tag{2.2}$$

which yields (2.3):

$$n = \frac{\ln(0.5)}{\ln(\cos(\theta_{1/2}))}. \tag{2.3}$$

Assuming that the LED intensity pattern can be approximated by the generalized Lambertian model, the equation which describes optical power P_{Tx} emitted by an LED into the hemisphere can be written as (2.4):

$$I_{\mathrm{Tx}}(\theta) = \frac{n+1}{2\pi} P_{\mathrm{Tx}} \cos^n(\theta) \qquad \text{for} \quad \theta \ \epsilon \ [-\pi/2, \pi/2]. \tag{2.4}$$

The coefficient $(n+1)/2\pi$ ensures that integrating $I_{\mathrm{Tx}}(\theta)$ over the solid angle of the hemisphere results in the source power P_{Tx}. In order to simplify the notation, the general transmitter function H_{Tx} derived from (2.4) is further denoted as follow (2.5):

$$H_{\mathrm{Tx}}(n, \theta) = \frac{n+1}{2\pi} \cos^n(\theta) \qquad \text{for} \quad \theta \ \epsilon \ [-\pi/2, \pi/2]; \ \vec{n}_{\mathrm{Tx}}, \tag{2.5}$$

where $\vec{n}_{\mathrm{Tx}}$is emitter normal vector [6, 4, 15].

2.1.2 Reflection model

Reflection and/or diffusion occurs when the transmitted light wave meets a surface whose dimensions are larger when compared to the wavelength. The nature of the reflection depends on several factors, in particular the surface roughness, the angle of incidence and wavelength. Basically, there are two types of reflection related to wavelength of incident radiation which can be considered: i) specular reflection, for perfectly smooth surfaces; and ii) diffuse specular reflection, for surfaces with some degree of roughness. The nature of diffuse specular reflections depends on the angle of incidence wave and have elaborate models. On the other hand, ideally, diffuse reflectors can be modeled as pure Lambertian sources. Diffuse reflectors are approximated using Lambert's model which yields the following reflection function R_{Lambert} (2.6):

$$R_{\mathrm{Lambert}}\left(\rho, \Delta A, \left\|d_{\mathrm{I}}^{\vec{\mathrm{Ref1}}}\right\|, \alpha, \beta\right) = \frac{\rho \Delta A}{\pi \left\|d_{\mathrm{I}}^{\vec{\mathrm{Ref1}}}\right\|^2} \cos(\alpha) \cos(\beta) \qquad \text{for} \quad \vec{\mathrm{n}}_{\mathrm{Ref}}, \tag{2.6}$$

where R_{Lambert} represents reflection function, ρ is the surface reflection coefficient, $d_{\mathrm{I}}^{\vec{\mathrm{Ref1}}}$ and $\left\|d_{\mathrm{I}}^{\vec{\mathrm{Ref1}}}\right\|$ represents the incident direction and distance, respectively. Symbol ΔA is the surface element area and α , β are angles of incidence and reflection, respectively.

2.1.3 Receiver model

The detected signal impinges a photo-detector active area A_{Rx} after traveling a distance expressed by $\left\|\vec{d_{\mathrm{Rx}}}\right\|$ $\left(\text{with } A_{\mathrm{Rx}} \ll \left\|\vec{d_{\mathrm{Rx}}}\right\|^2\right)$ between transmitter and receiver.

In order to simplify the channel model notation, the generalized function of the receiver H_{Rx} can be written as (2.7):

$$H_{\mathrm{Rx}}\left(\left\|\vec{d_{\mathrm{Rx}}}\right\|, \ \psi\right) = \frac{T(\psi) g(\psi) A_{\mathrm{Rx}}}{\left\|\vec{d_{\mathrm{Rx}}}\right\|^2} \cos(\psi) \operatorname{rect}\left(\frac{\psi}{FOV}\right) \qquad \text{for} \quad \vec{\mathrm{n}}_{\mathrm{Rx}}, \tag{2.7}$$

where ψ is the viewing angle of the receiver, $T(\psi)$ is the filter transmission, $g(\psi)$ concentrator gain, *FOV* is the receiver field of view, $\vec{n}_{\mathrm{Rx}}$ is the receiver normal vector and the rect(x) function is the receiver *FOV* bounding function, given by (2.8).

$$\mathrm{rect}(x) = \begin{cases} 1 \in |x| \leq 1 \\ 0 \in |x| > 1 \end{cases}. \tag{2.8}$$

2.2 ODAC-based VLC system performance investigation

Geometrical arrangement, an appropriate LED array topology and bit resolution play key roles in overall performance of the VLC system employing the ODAC-based transmitter. Thus, the following simulation examines error performance of five formerly proposed ODAC LED arrays. It was assumed that the VLC system under consideration operated with one dominant wavelength, i.e. only the blue component participated in the communication (slow yellowish re-emitted component was filtered on the receiver side).

Figure 2.1 depicts system conceptual diagram considering only a direct LoS communication path to examine LED arrays in terms of bit depth and array topology. On the transmitter side, an arbitrary waveform generator (AWG) produced a digital signal $v(t)$, represented by a set of k digital bit streams $B(t)$, which were used to modulate k independent groups of LEDs in an LED array. Quantization at the transmitter side was assumed to follow the standard approach: for k LED groups, the signal dynamic range was divided into $2^{\mathrm{k}} - 1$ equal amplitude intervals. Assuming that the digital signals $B(t)$, all had the same amplitude and that the LEDs were driven uniformly for all k groups, the digital weights were set by the number of LEDs in each group, that is, following a binary weight distribution. The transmitted bit streams were then combined on the optical channel and reach the input of the receiver (in this case, represented by a simple transimpedance amplifier (TIA) . The recovered signal $\bar{v}(t)$ was a reconstructed replica of $v(t)$ with approximation error dependent on the bit depth of the array (the number of LED groups, k) and the LED array topology. In a perfect channel, exempt from reflections, delays and constrained *FOV*, the approximation error would be lower bounded by LSB/2, where the least significant bit (LSB) represented the strength of the least significant bit.

Figure 2.1: Conceptual system diagram

Assuming that the channel impulse response of a single LED is expressed by $h(t)$, the recon-

structed signal can be determined by adding the convolutions of the signals $B(t)$ with the LED's individual impulse responses, as stated in (2.9):

$$\bar{v}(t) = R_{\mathrm{PD}} P_0 \sum_{\mathrm{m}=1}^{\mathrm{k}} \sum_{\mathrm{n}=1}^{2^{\mathrm{m}-1}} B_{\mathrm{m}}(t) \star h_{\mathrm{m,n}}(t), \tag{2.9}$$

where P_0 is total optical power, the PD was modeled with active area A_{Rx} and responsivity R_{PD}, m denotes order of the LED group in the LED array and n is associated with the number of LEDs for each group m. For slow varying signals, the channel impulse response has negligible impact on signal reconstruction. For these cases, equation (2.9) can be simplified, assuming that the contribution from the LoS path and the multiple reflections add together at an instant of time, and CIR $h(t)$ is a single Dirac impulse,with strength given by the addition of the DC channel gain H in this case only from the direct LoS path, as follow (2.10):

$$\bar{v}(t) = R_{\mathrm{PD}} P_0 \sum_{\mathrm{m}=1}^{\mathrm{k}} \sum_{\mathrm{n}=1}^{2^{\mathrm{m}}-1} B_{\mathrm{m}}(t) H_{\mathrm{m,n}}. \tag{2.10}$$

The DC channel gain for each LED in the array H can be directly computed as LoS contribution H^{LoS} using equations (2.4) and (2.7) according to equation (2.11),

$$H = H^{\mathrm{LoS}} = H_{\mathrm{Tx}}(n, \theta) H_{\mathrm{Rx}}\left(\left\|\vec{d}_{\mathrm{Rx}}\right\|, \psi\right). \tag{2.11}$$

Equation (2.10) states that for slowly varying signals the approximated signal error depends only on the geometrical features of the set-up, including the *FOV* receiver, the *HPA* LED, the distance between transmitter and receiver, and the presence of reflecting elements. It is necessary to say that the proposed model neglected influence of any noise contributors in order to explore formerly mentioned geometrical dependencies.

As a suitable performance metric able to evaluate signal reconstruction error, the relative root mean square error E_{RMS} was chosen. The normalized versions of transmitted signal $v(t)$ and recovered signal $\bar{v}(t)$ on the receiver side were assumed. ODAC performance assessment used periodic signals to simplify comparison between the original signal and the recovered one. It was assumed that the receiver will start working immediately as the first signals hit the photo-detector. It was necessary to consider the delayed replica of the original signal to have a fair error evaluation. In this case, a delayed replica of the original signal $v(t-\Delta t)$ was used for this purpose. The term Δt is the minimum delay measured for each receiver position, that is, corresponding to the smallest direct path between transmitters and receiver. The term T corresponds to a signal period. The relative root mean square error E_{RMS} is then expressed by equation (2.12).

$$E_{\mathrm{RMS}} = \frac{\sqrt{\frac{1}{T}\int_{\Delta t}^{T+\Delta t} \left(v(t-\Delta t) - \overline{v}(t)\right)^2 \mathrm{d}t}}{\sqrt{\frac{1}{T}\int_{\Delta t}^{T+\Delta t} \left(v(t-\Delta t)\right)^2 \mathrm{d}t}}. \tag{2.12}$$

Figure 2.2 depicts on-axis E_{RMS} dependence on distance x ($y = 0$) between transmitter and receiver. It was assumed that the optical signal travels directly to the receiver having *FOV* 60° with responsivity $R_{\mathrm{PD}} = 0.8$ V/W. It is apparent that near field optical intensity inhomogenity resulted in error in front of the transmitter. It can be extracted that the narrow LED *HPA* resulted in enormous E_{RMS} for near field area. Moreover, insufficient transmitter resolution was a consequence of another excessive error. However, compact PLCC6 LED array dimensions posed certain improvement in front of the transmitter and even over the full length. Figure 2.3 depicts E_{RMS} performance for the receiver being swept over the rectangle area of 6m x 2m. As can be seen, the results demonstrate E_{RMS} performance in terms of angular displacement and confirms previous error performance behavior for confined LED *HPA*s.

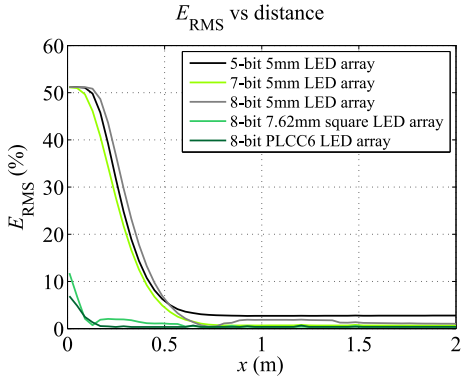

Figure 2.2: On axis E_{RMS} performance

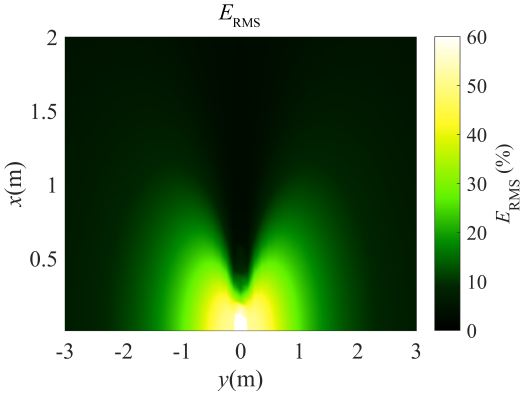

(a) 5-bit 5mm LED array E_{RMS} (*HPA* 15°, *FOV* 60°)

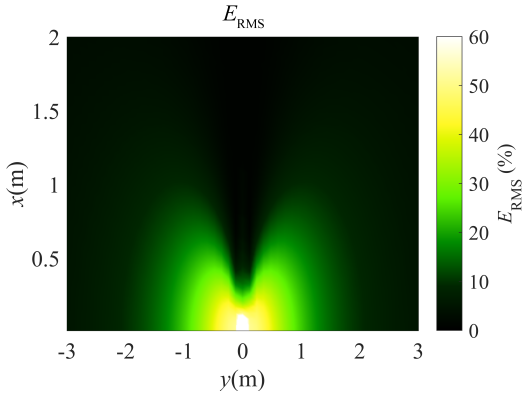

(b) 7-bit 5mm LED array E_{RMS} (*HPA* 15°, *FOV* 60°)

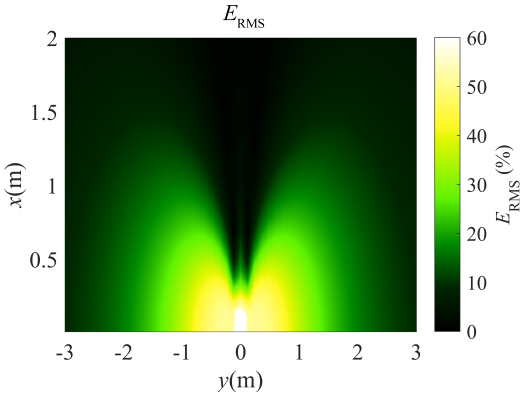

(c) 8-bit 5mm LED array E_{RMS} (*HPA* 15°, *FOV* 60°)

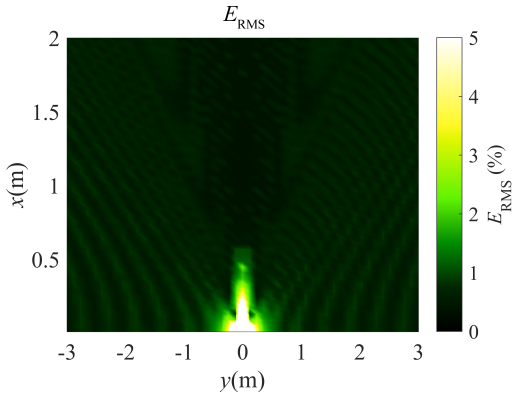

(d) 8-bit 7.62mm LED array E_{RMS} (*HPA* 90°, *FOV* 60°)

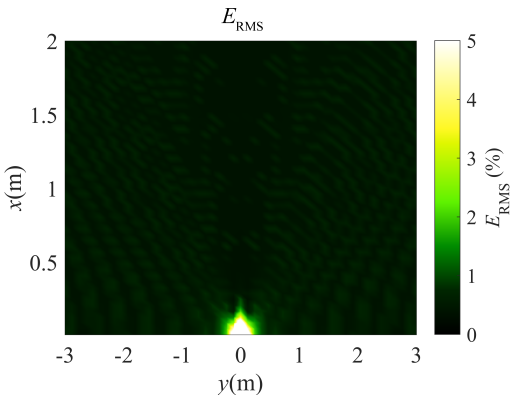

(e) 8-bit PLCC6 LED array E_{RMS} (*HPA* 60°, *FOV* 60°)

Figure 2.3: Spatial E_{RMS} performance

2.3 Multi-path signal propagation model

Figure 2.4 depicts the multi-path system set-up considering one reflection path. The transmitter comprises the LED array, assembled at a height h_{Tx} above ground (xy plane), with heading defined by the normalized vector $\vec{n}_{\mathrm{Tx}}$. The optical signal traveled through the optical channel between transmitter and receiver, undergoing path attenuation and reflections from the ground surface. For simulation purposes a single reflection scenario from the ground was assumed. The reflection coefficient was set to $\rho = 0.15$, the single reflection presented a dark ground with a high absorption (worn asphalt was assumed). The receiver was positioned equidistantly at different places in plane xy, with a height h_{Rx} above ground and normalized vector $\vec{n}_{\mathrm{Rx}}$ pointing always to the center of the LED array. The DC channel gain for each LED in array H can be separated into two components; the first due to the LoS H^{LoS} contribution and the second one H^{Ref1} due to multiple reflections on the ground surface, given by (2.13).

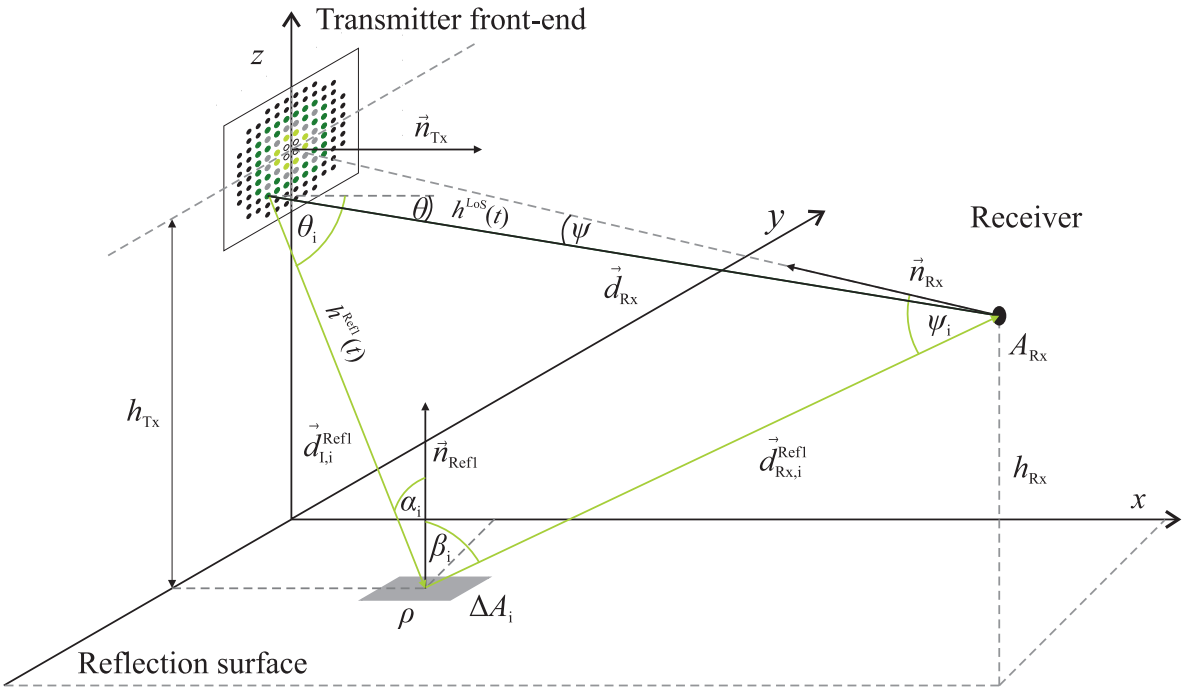

Figure 2.4: Detailed multi-path system set-up

$$H = H^{\mathrm{LoS}} + H^{\mathrm{Ref1}}. \tag{2.13}$$

The gain of the signal arriving to the receiver through the first reflected path H^{Ref1} can be computed using equations (2.4), (2.7) and the appropriate reflection model, in this case Lambertian, R_{Lambert} given by equation (2.6), which yields (2.14). For the scenario under consideration, worn asphalt was modeled as a pure Lambert radiator.

$$H^{\mathrm{Ref1}} = \sum_{\mathrm{i}=1}^{G_{\mathrm{Ref1}}} H_{\mathrm{Tx}}(n,\theta_{\mathrm{i}})\, H_{\mathrm{Rx}}\left(\left\|\vec{d}^{\,\mathrm{Ref1}}_{\mathrm{Rx,i}}\right\|, \psi_{\mathrm{i}}\right) R_{\mathrm{Lambert}}\left(\rho, \Delta A_{\mathrm{i}}, \left\|\vec{d}^{\,\mathrm{Ref1}}_{\mathrm{I,i}}\right\|, \alpha_{\mathrm{i}}, \beta_{\mathrm{i}}\right), \tag{2.14}$$

where G_{Ref1} specifies the number of grid elements ΔA used to approximate the reflection contributions from the ground surface, $\left\|\vec{d}^{\,\mathrm{Ref1}}_{\mathrm{I}}\right\|$ stands for the distance from the transmitter to the first reflection surface, $\left\|\vec{d}^{\,\mathrm{Ref1}}_{\mathrm{Rx}}\right\|$ states for the distance from the first reflection surface to the receiver and index i is associated with the number of first reflection paths. Finally, the reconstructed signal can be computed using equation (2.10), thus combining the contribution of every LED in the array, plus the geometrical dependencies of the optical signal propagation.

The relative root mean square error E_{RMS} was selected as the performance metric suitable to the previously used to evaluate the reconstruction error in the VLC system using the ODAC concept. For that purpose the scaled versions $v(t)$ and $\overline{v}(t)$ of the original and reconstructed signals, respectively, were considered. Performance evaluation was based on periodic signals in order to simplify the comparison between the original and reconstructed signal versions.

As indicated in equation (2.12) the relative root mean square error E_{RMS} will depend on the positioning of the receiver with respect to the transmitter. The 5mm conventional LEDs under consideration used narrow *HPA* of 15° (suitable for higher communication distances thanks to their high directivity) and total optical power P_0. The effect of the *FOV* for testing purposes was considered taking 30° and 60°. The figures 2.5 and 2.6 show the results for the far field VLC scenario (xy plane 10m x 20m) with the two different LED arrays 5 and 8-bit, respectively. The performance comparison between the LoS scenario and one reflection scenario for 5-bit set-up was made. The simulation proved that an indirect path improves the system performance in front of the transmitter, assuming slow data rates. Furthermore, figures 2.5c and 2.5d show the effect of receiver *FOV*. The achieved results showed that the minimum achieved error is 7.3% and 0.8%, for the 5 and 8-bit depth arrays, respectively. Obviously, the error E_{RMS} decreased with bit depth likewise in the case of electrical DACs (EDACs). As can be expected, the error area in the transmitter near field proportionally increased with the number of LEDs in the array which is a natural consequence of larger emitter dimensions. The error performance in front of the transmitter may also be further improved by increasing the LED placement density inside the LED array. Based on preliminary results, the 8-bit ODAC emitter seems to be the most suitable option for the next study. Thus, the next steps dealing with channel impulse response employ merely 8-bit ODAC front end versions [6].

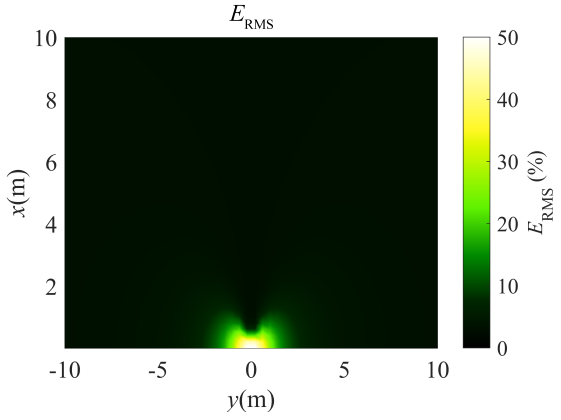

(a) 5-bit 5mm LED array E_{RMS} (LoS, *HPA* 15°, *FOV* 30°)

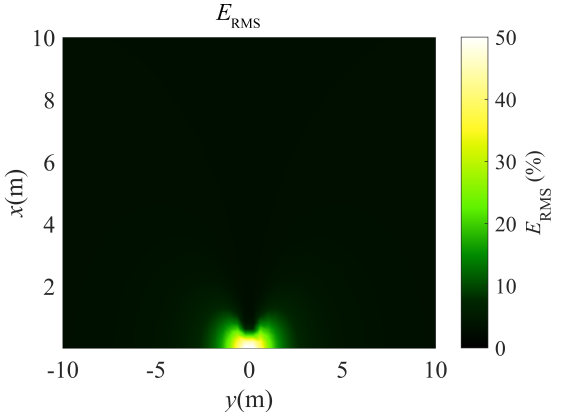

(b) 5-bit 5mm LED array E_{RMS} (LoS, *HPA* 15°, *FOV* 60°)

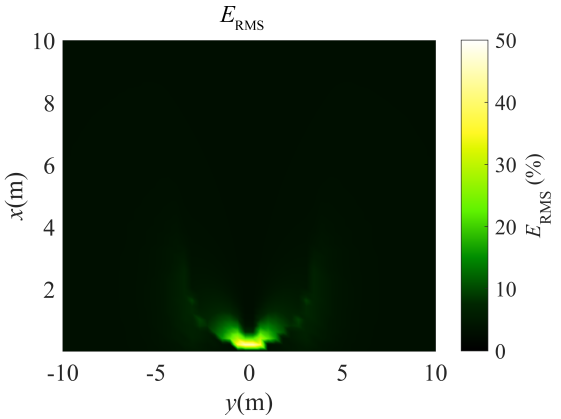

(c) 5-bit 5mm LED array E_{RMS} (LoS+Ref1, *HPA* 15°, *FOV* 30°)

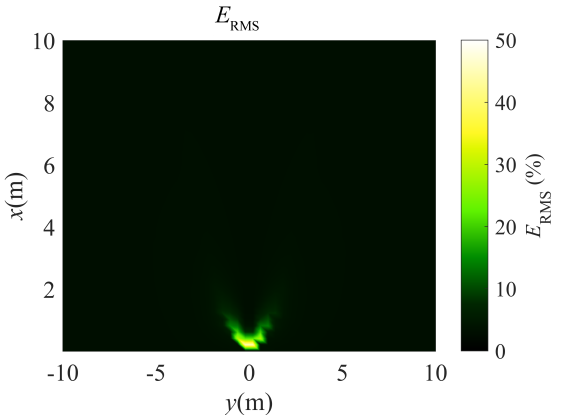

(d) 5-bit 5mm LED array E_{RMS} (LoS+Ref1, *HPA* 15°, *FOV* 60°)

Figure 2.5: E_{RMS} performance comparison of 5-bit LED arrays

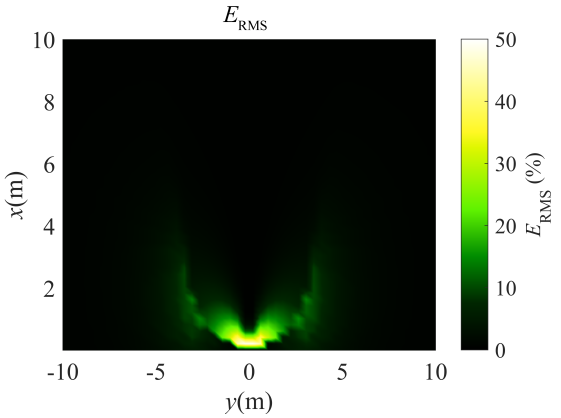

(a) 8-bit 5mm LED array E_{RMS} (LoS+Ref1, *HPA* 15°, *FOV* 30°)

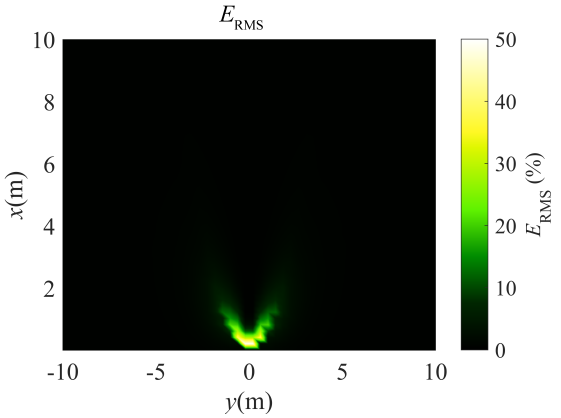

(b) 8-bit 5mm LED array E_{RMS} (LoS+Ref1, *HPA* 15°, *FOV* 60°)

Figure 2.6: E_{RMS} performance of 8-bit LED arrays

2.4 Study on utilizing the ODAC concept in ITS applications

Figure 2.7 depicts a system model of I2V VLC using ODAC-based LED traffic lights placed into a standardized 300mm signal head case. The emitter consisted of multi-unit signal heads comprising the near right-side head at a height 2.1m and the through head placed at 5.2m above the xz ground plane. The illustrated traffic lights placement complies with standards ČSN 36 5601-1 and ČSN 73 6021 [1, 2].

The road dimensions meet the standard ČSN 73 6110, more specifically, the ground plane width x was set to 6.5m and the road length z under consideration to 30m illustrated as a red-colored rectangle [3]. Moreover, the proposed road area represented a reflection surface for the following simulation purposes. A blue-colored rectangle depicted in figure 2.7 illustrates a receiver plane at height 0.7m corresponding to headlight height of a typical vehicle.

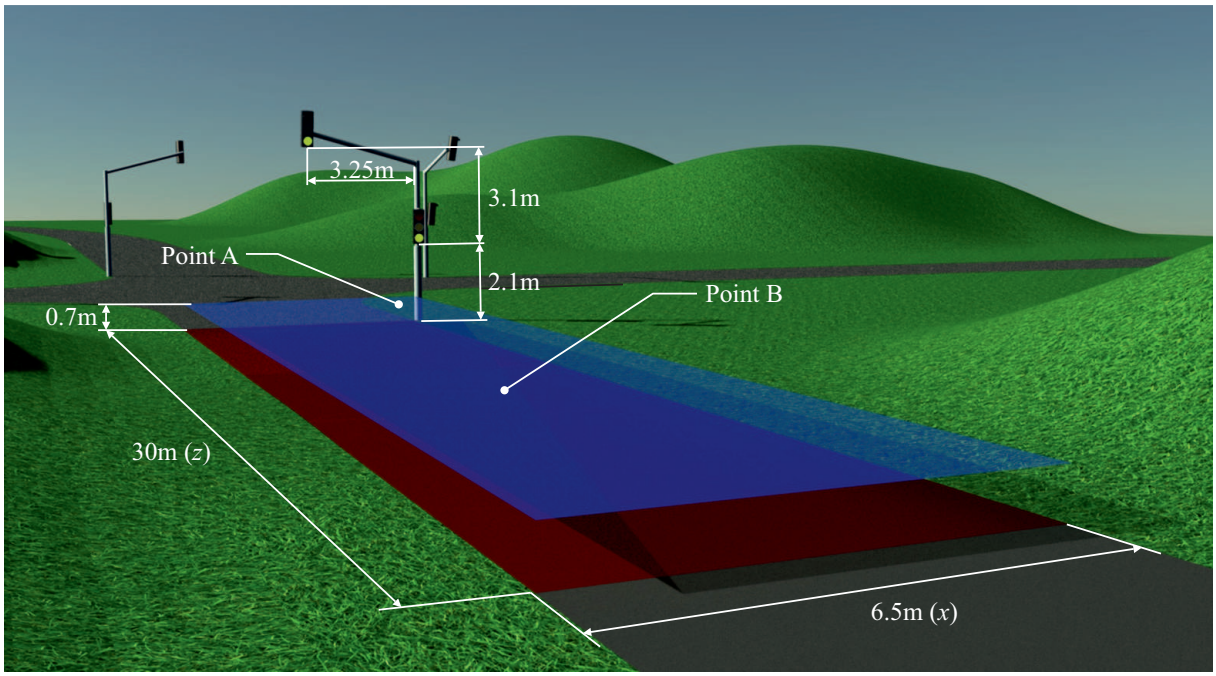

Figure 2.7: Crossroad model

The foregoing analysis assumed that a single wavelength was used for communication purposes. The devised set-up considered two 8-bit 5mm LED arrays. Each LED array was composed of LED groups which represented the bit depth of the array. The number of LEDs inside the array was directly given by $2^k - 1$, due to a symmetrical axis. The transmitter used two LED arrays with dominant wavelength 505nm, assembled at a height of 2.1m and 5.5m above ground (xz plane), with heading defined by the vector $\vec{n}_{\text{Tx}}$. Green lights of the traffic head were chosen in order to simplify the simulation. All the LED arrays transmitted the same information synchronously. The optical signal traveled through the optical channel between transmitter and receiver, undergoing path attenuation and reflections from the ground. For simulation purposes, a single reflection scenario from the ground surface was assumed. The reflection coefficient was set to $\rho = 0.08$, equal to the reflection coefficient of a worn asphalt surface, assuming a wavelength at 505nm [14]. The receiver was positioned at different places inside a rectangular ground plane 6.5m by 30m with a heading vector $\vec{n}_{\text{Rx}}$as illustrated in figure 2.7. The CIR of a single LED $h(t)$ can be separated into two components, the first one due to the LoS contribution, and the second owing to the first order reflections on the ground surface.

$$h(t) = h^{\text{LoS}}(t) + h^{\text{Ref1}}(t). \tag{2.15}$$

The LoS contribution $h^{\text{LoS}}(t)$ can be computed directly using equation (2.16):

$$h^{\text{LoS}}(t) = H_{\text{Tx}}(n,\theta) H_{\text{Rx}}\left(\left\|\vec{d}_{\text{Rx}}\right\|, \psi\right) \delta\left(t - \Delta t_{\text{LoS}}\right), \tag{2.16}$$

where $\delta(.)$ represents the Dirac delta function, Δt_{LoS} is time delay of the path between the trans-

mitter and receiver given by the length of the path divided by the propagation speed (in this case, the speed of light). The signal arriving at the receiver after one reflection can be computed using equations (2.7), (2.5) and the reflection model R_{Lambert} given by equation (2.6). For the scenario under consideration, the ground surface was modeled as a pure Lambertian surface. The contribution from the first reflection path $h^{\text{Ref1}}(t)$ is expressed by (2.17):

$$h^{\text{Ref1}}(t) = \sum_{\text{s1}} \sum_{\text{i}=1}^{G_{\text{Ref1}}} H_{\text{Tx}}(n, \theta_{\text{i}}) H_{\text{Rx}}\left(\left\| d_{\text{Rx,i}}^{\vec{\text{Ref1}}} \right\|, \psi_{\text{i}}\right) \times R_{\text{Lambert}}\left(\rho, \Delta A_{\text{i}}, \left\| d_{\text{I,i}}^{\vec{\text{Ref1}}} \right\|, \alpha_{\text{i}}, \beta_{\text{i}}\right) \delta\left(t - \Delta t_{\text{Ref1,i}}\right), \quad (2.17)$$

where s1 specifies the number of reflection surfaces under consideration (for this purpose s1=1), G_{Ref1} specifies the number of grid elements ΔA used to approximate the reflection contributions and Δt_{Ref1} is the time delay associated with the path between transmitter, reflecting surface and receiver, computed as before.

As a proven performance metric to evaluate the signal reconstruction, the relative root mean square error E_{RMS} was used as stated in (2.12). The testing signal $v(t)$ was modeled by a sampled sinusoidal waveform with frequencies 1MHz and 10MHz. The sample rate of the generated signal complied with the Nyquist criterion. Figure 2.8 shows the general DC channel gain H_{G} expressed by (2.18) where a means the number of all transmitter arrays under consideration (in this case two emitter arrays).

$$H_{\text{G}} = \sum_{\text{a}} \sum_{\text{m}=1}^{\text{k}} \sum_{\text{n}=1}^{2^{\text{m}-1}} \left(H_{\text{m,n}}^{\text{LoS}} + H_{\text{m,n}}^{\text{Ref1}}\right). \quad (2.18)$$

Figure 2.9 shows the reconstruction error distribution over the receiver plane (blue rectangle in figure 2.7) for different emitter *HPA* and receiver *FOV*. Results, for signal frequency 1MHz and 10MHz, displayed larger error in front of the receiver. This is a natural property of the ODAC concept inducing distortion in the near field of the ODAC LED array. Higher emitter *HPA* positively influenced the reconstruction error especially close to the traffic heads as depicted in 2.9b and 2.9d. Needless to say, the signal frequency itself increased the overall reconstruction error. Noticeable error fringes, in all figures, were a product of signal interference in the optical domain between the two traffic head emitters. [8].

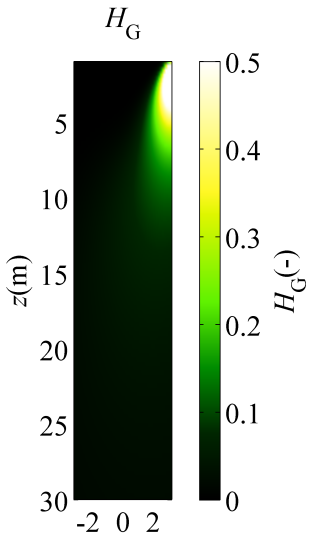

(a) H_G, *HPA* = 15°, *FOV* 60°

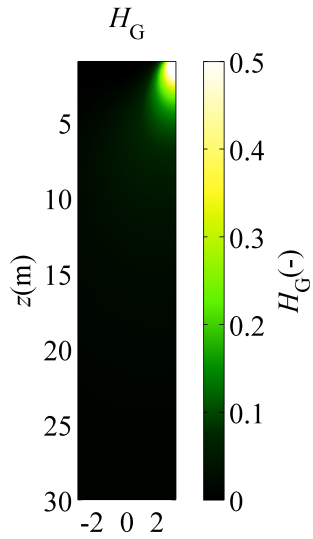

(b) H_G, *HPA* = 30°, *FOV* 60°

Figure 2.8: General DC channel gain H_G

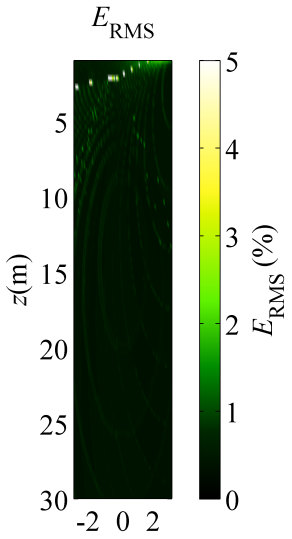

(a) 1MHz *HPA* = 15°, *FOV* 60°

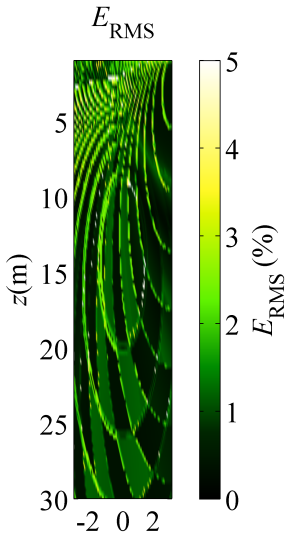

(b) 10MHz *HPA* = 15°, *FOV* 60°

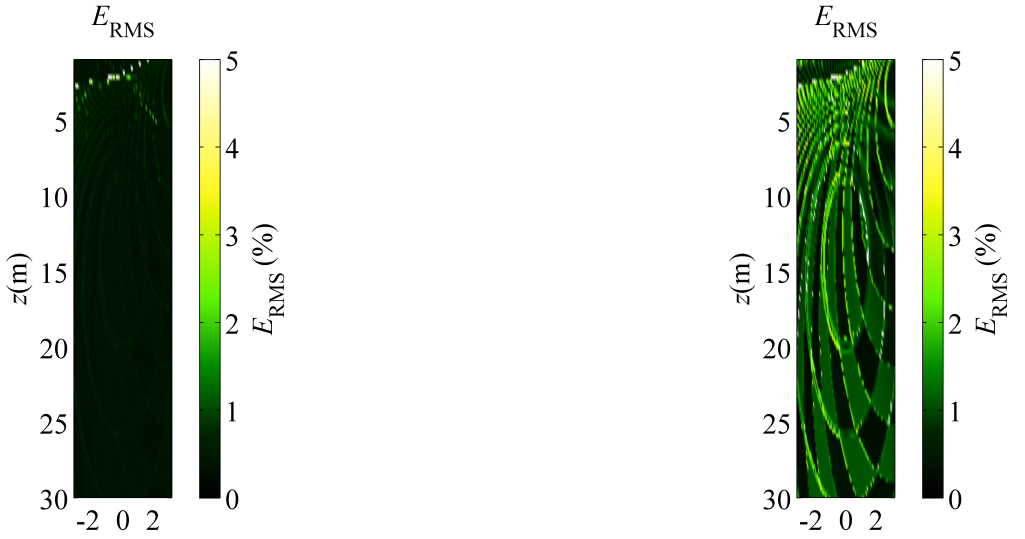

(c) 1MHz *HPA* = 30°, *FOV* 60°

(d) 10MHz *HPA* = 30°, *FOV* 60°

Figure 2.9: Signal reconstruction error E_{RMS}

Figure 2.10 shows the signal reconstruction error for determined points at the receiver plane (Point A and point B drawn in figure 2.7).

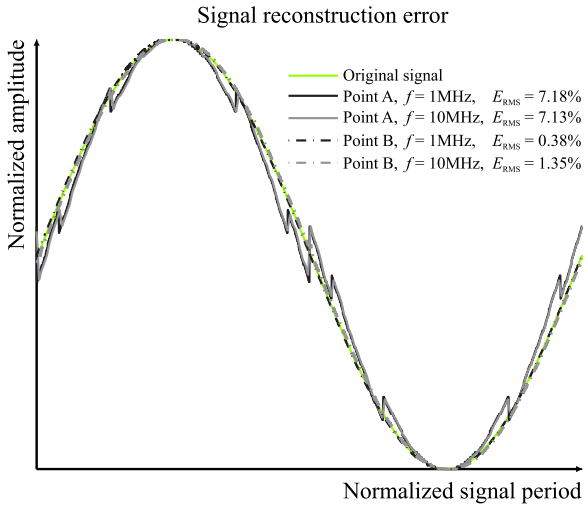

Figure 2.10: Reconstruction error (*HPA* = 30°, *FOV* 60°)

2.5 ODAC system performance analysis for indoor set-up conditions

This part explores ODAC performance degeneration effects caused by the geometrical set-up and CIR for indoor conditions. In former sections relating to this topic, the effects on signal reconstruction error due to geometrical considerations of the set-up, assuming low data transmission scenarios, were investigated [6, 7]. The outdoor VLC model of the ITS crossroad using a similar performance evaluation metric was revealed in [8]. This section extends previous conclusions to the case of high

data rate signal transmission, where the channel impulse response becomes of paramount importance. The assumed set-up scenario considered four luminaries in an empty room of 4mx4mx3m (length, width, and height). The modeling approach took into consideration the effects of the emitter *HPA*, the receiver *FOV* and channel impulse response, assuming a multi-path propagation model able to consider up to two reflection paths.

A detailed geometrical set-up under consideration can be seen in figure 2.11. On the transmitter side, an arbitrary waveform generator produced a digital signal $v(t)$, represented by a set of k digital bit streams $B(t)$, which were used to modulate k independent groups of LEDs in an LED array. Quantization at the transmitter side was assumed to follow the standard approach: for k LED groups, the signal dynamic range was divided into $2^k - 1$ equal amplitude intervals. Assuming that the digital signals $B(t)$, all had the same amplitude and that the LEDs were driven uniformly for all the k groups, the digital weights were set by the number of LEDs in each group - following a binary weight distribution.

The transmitted bit streams were then combined on the channel and reach the input of the receiver (in this case, represented by PD and simple TIA). The recovered signal $\overline{v}(t)$ was a reconstructed replica of $v(t)$ with approximation error dependent on the bit depth of the array (the number of LED groups, k), and channel degradation effects. In a perfect channel, exempt from reflections, delays and constrained *FOV*, the approximation error would be lower bounded by LSB/2, where LSB represented the strength of the least significant bit. Assuming the channel impulse response $h(t)$ of one LED , the reconstructed signal could be determined by adding the convolutions of the signals $B(t)$ with the LED's individual impulse responses, as stated in (2.9).

As stated in equation (2.9) the reconstruction error will depend on the optical channel, this implies dependence on the CIR, the geometrical arrangement between transmitter and receiver, and the presence of reflecting elements. The assumed set-up considered four 8-bit depth LED array luminaries. Each LED array was formed by k LED groups, where k represents the bit depth of the array. Inside each group, the number of LEDs depended on the symmetries of the topology. For one axis symmetric 8-bit depth LED arrays, the overall number of LEDs inside the array was directly given by $2^k - 1$. For the present case, the number of LEDs inside each array was 255 (bit 0 =1 LED, bit 1 = 2 LEDs, bit 3 = 4 LEDs, (...), bit 7 = 128 LEDs), having a single symmetrical axis.

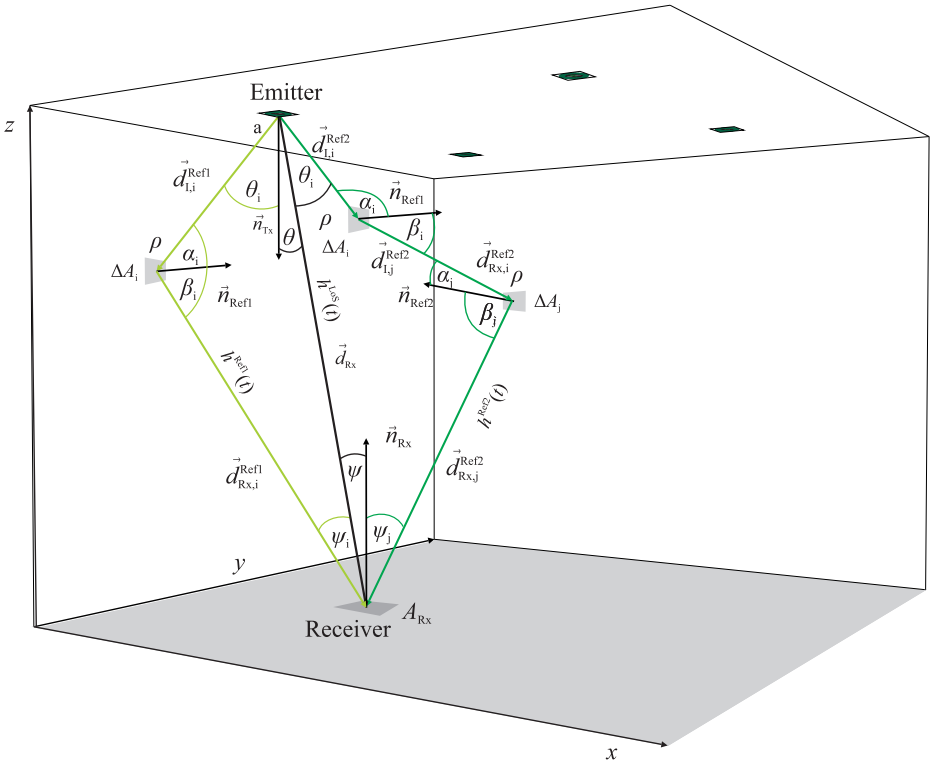

Figure 2.11: Detailed set-up

The transmitter used four LED arrays, located at a height z (3m) above the ground plane (xy plane), with heading given by the normalized vector $\vec{n}_{\mathrm{Tx}}$. All LED emitters under consideration sent the same information synchronously. The optical signal which went through the optical channel was affected by path attenuation and reflection from the walls. Simulation assumed a double reflection scenario from surrounding walls and the ceiling. The reflection coefficient of dominant wavelength 475 nm was set to $\rho = 0.8$, which corresponds to white paint on a plaster surface [19]. The receiver was swept at 10,000 different positions inside a 4m by 4m square on the ground plane ($z = 0$), with a heading vector $\vec{n}_{\mathrm{Rx}}$. The CIR $h(t)$ can be divided into three components; the first one owing to the LoS contribution, the second and third, due to the first and second order reflections from walls, respectively.

$$h(t) = h^{\mathrm{LoS}}(t) + h^{\mathrm{Ref1}}(t) + h^{\mathrm{Ref2}}(t). \tag{2.19}$$

The LoS contribution $h^{\mathrm{LoS}}(t)$ can be directly computed using equation (2.16). The signal impinging the receiver after the first reflection is possible to compute using equations (2.17) and including a suitable reflection model. For simulation purposes, a white plaster wall was modeled as a pure Lambertian radiator. The second reflection contribution can be expressed using the same analogy as in the former case. The second reflection contribution $h^{\mathrm{Ref2}}(t)$ is given by equation (2.20).

$$h^{\mathrm{Ref2}}(t) = \sum_{\mathrm{s1}}\sum_{\mathrm{s2}}\sum_{\mathrm{i}=1}^{G_{\mathrm{Ref1}}}\sum_{\mathrm{j}=1}^{G_{\mathrm{Ref2}}} H_{\mathrm{Tx}}(n,\theta_{\mathrm{i}})\, H_{\mathrm{Rx}}\left(\left\|\vec{d}^{\,\mathrm{Ref2}}_{\mathrm{Rx,j}}\right\|, \psi_{\mathrm{j}}\right) R_{\mathrm{Lambert}}\left(\rho, \Delta A_{\mathrm{i}}, \left\|\vec{d}^{\,\mathrm{Ref2}}_{\mathrm{I,i}}\right\|, \alpha_{\mathrm{i}}, \beta_{\mathrm{i}}\right) \times$$
$$R_{\mathrm{Lambert}}\left(\rho, \Delta A_{\mathrm{j}}, \left\|\vec{d}^{\,\mathrm{Ref2}}_{\mathrm{I,j}}\right\|, \alpha_{\mathrm{j}}, \beta_{\mathrm{j}}\right) \delta\left(t - \Delta t_{\mathrm{Ref,ij}}\right), \quad (2.20)$$

where s2 specifies the number of reflection surfaces undergoing the second order reflection, G_{Ref2} specifies the number of second order grid elements, $\vec{d}^{\,\mathrm{Ref2}}_{\mathrm{I}}$ means incident direction of the second order reflection, $\vec{d}^{\,\mathrm{Ref2}}_{\mathrm{Rx}}$ is the direction from the second reflection surface to the receiver, Δt_{Ref2} is the time delay associated with the path between transmitter, reflecting surfaces and receiver, and index j is associated with the number of second reflection paths, computed as before.

The numerical computation process can be conveniently modified in order to investigate the symmetric nature of the set-up. Hence, symmetric configurations required simulation of one luminaire, where the other luminaires were rotated replicas of the first. Eventually, the recovered signal could be obtained using equation (2.9). Particularly, the signal was a combination of the contribution from each LED in the array and geometrical dependencies of the optical signal propagation. The procedure to compute CIR followed the standard time histogram approach, where each time bin accumulated all contributions with similar delay. The time bin resolution of the CIR was in this way linked to the area grids used for reflection modeling, having in mind that each bin interval must satisfy the constraint $c\Delta t > \sqrt{\Delta A}$ [4]. In practice, a CIR computation for simulation purposes was based on a modified iterative algorithm arising from Barry's study on CIR modeling implemented by using MATLAB software. More specifically, the MATLAB parallel computing toolbox, in this case using 10 pools, was employed in order to reasonably carry out demanding CIR computations of the second reflection order for 10,000 reflection elements and receiver positions.

In wireless communication systems the *EVM* is perhaps the most common figure of merit. In this case, *EVM* was chosen as the suitable metric to evaluate the overall performance of the setup under consideration. Needless to say, the setup does not include any modulation scheme, as commonly found in RF transceiver performance testing. The evaluation rather used *EVM* as a measure of difference between the measured signal and the reference signal, as defined in equation (2.21). Basically, *EVM* corresponds to previously used E_{RMS}, The normalized reference signal $v(t)$ and the recovered signal $\overline{v}(t)$ on the receiver side were assumed. The time offset and frequency offset was removed where M is data length.

$$EVM = \sqrt{\frac{\sum_{t=1}^{\mathrm{M}} \left\|\overline{v}(t) - v(t)\right\|^2}{\sum_{t=1}^{\mathrm{M}} \left\|v(t)\right\|^2}}. \quad (2.21)$$

The simulation set-up assumed the modeling approach described in the previous sections of the thesis. The signal $v(t)$ was modeled by a quantized sinusoidal waveform with frequencies ranging

from 1MHz to 100MHz. The sample rate of the generated signal was set to comply with the Nyquist criterion, in this case to 10GHz. Obviously this is not achievable with present commercial LEDs but it may disclose some relevant considerations for devices currently under development (mLEDs bring bandwidth up to 400MHz). The achieved results are depicted in figures 2.12 to 2.13.

Figures 2.12 and 2.13 show the general DC channel gain H_{G}, here defined as the sum of all LED CIRs from directed and reflected paths as stated in equation (2.22) and the reconstruction error distribution for the receiver in different positions over the ground plane. The *EVM* was computed using equation (2.21), for two different frequencies, 1MHz and 100MHz, with different transmitters *HPA*s and receivers *FOV*s. As in previous contributions, the DC channel gain depended strongly on *HPA* and *FOV*, having a major influence with larger *HPA*, meaning sources with wide radiation patterns. Usually this is the case for lighting systems where light uniformity is of paramount importance for better user comfort in terms of rendering conditions.

$$H_{\mathrm{G}} = \sum_{\mathrm{a}} \sum_{\mathrm{m}=1}^{\mathrm{k}} \sum_{\mathrm{n}=1}^{2^{\mathrm{m}-1}} \left(H_{\mathrm{m,n}}^{\mathrm{LoS}} + H_{\mathrm{m,n}}^{\mathrm{Ref1}} + H_{\mathrm{m,n}}^{\mathrm{Ref2}} \right), \tag{2.22}$$

where H^{Ref2} means DC channel gain of the second reflection path.

Figure 2.12 shows what can be expected for confined sources with reduced *HPA*. As can be seen, the reconstruction error did not change much for different receiver *FOV*s, which corresponded to better conditions for transmission. Also noticeable, there were some interference patterns arising from the multiple sources and reflecting surfaces, which became more evident for higher frequencies. These patterns resulted from wave interference phenomena, as for frequencies close to 100MHz, the wavelength became comparable to the room dimensions. Figure 2.13 shows the *EVM* for sources with high *HPA* (45º). For this case, the error dependence on the receiver *FOV*s was self-evident, showing different behaviors for 1MHz and 100MHz. This was due to the relevance of the delay terms for both frequencies. The errors also increased with frequency as before, but in this case the *EVM* reached nearly 50%. The main conclusion which can be extracted from these results is that under standard lighting conditions, communication impairments for systems employing the ODAC concept became relevant as the frequency increased. These problems can be mitigated by using photo-detectors with reduced *FOV*s or even concentrator lenses at the receiver side [9].

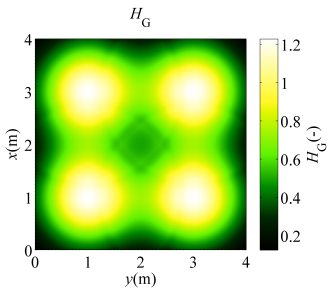

(a) DC gain *FOV* 30°

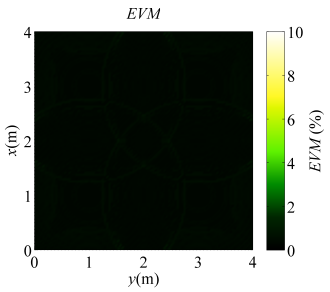

(b) *EVM*, f=1MHz, *FOV* 30°

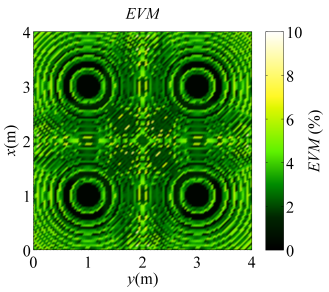

(c) *EVM*, f=100MHz, *FOV* 30°

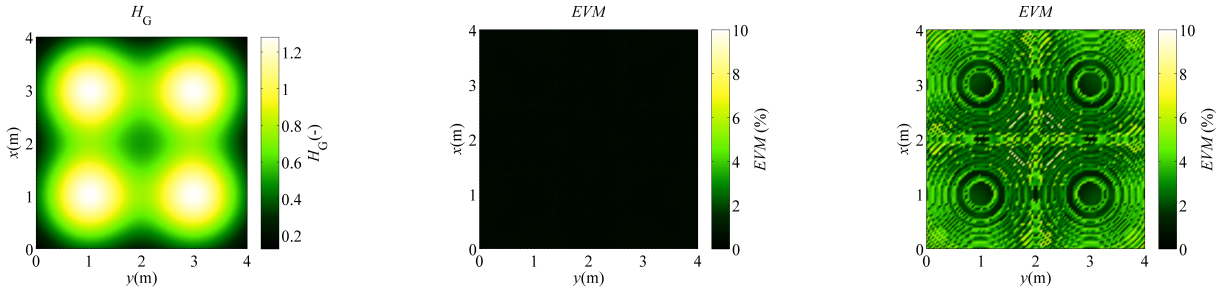

(d) DC gain *FOV* 60° (e) *EVM*, f=1MHz, *FOV* 60° (f) *EVM*, f=100MHz, *FOV* 60°

Figure 2.12: Four luminaires indoor set-up, *HPA* 15°

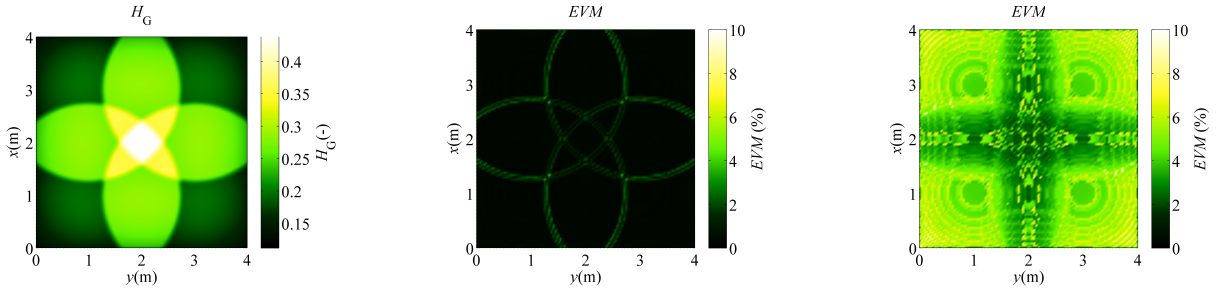

(a) DC gain *FOV* 30° (b) *EVM*, f=1MHz, *FOV* 30° (c) *EVM*, f=100MHz, *FOV* 30°

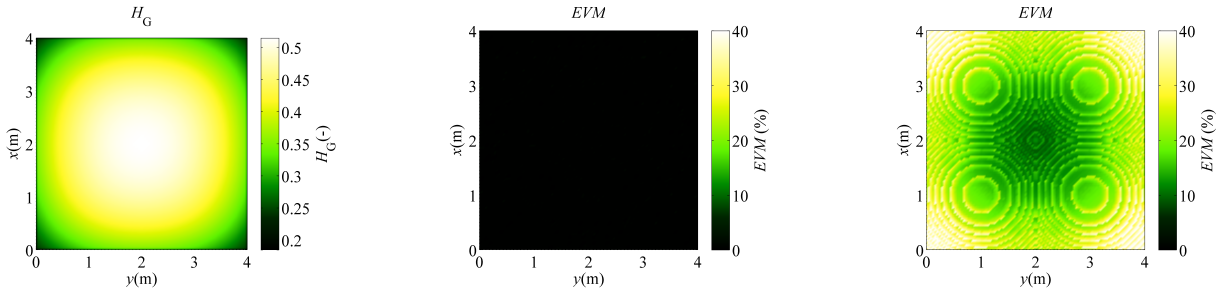

(d) DC gain *FOV* 60° (e) *EVM*, f=1MHz, *FOV* 60° (f) *EVM*, f=100MHz, *FOV* 60°

Figure 2.13: Four luminaires indoor set-up, *HPA* 45°

Figure 2.14b shows how the CIR affected the signal reconstruction for a 100MHz sinusoid at the three different receiver positions depicted in figure 2.14a (black dots inside the black circles). As explained before, the reconstruction error *EVM* was computed between the originally transmitted signal $v(t)$ and the reconstructed signal $\overline{v}(t)$ on the receiver side.

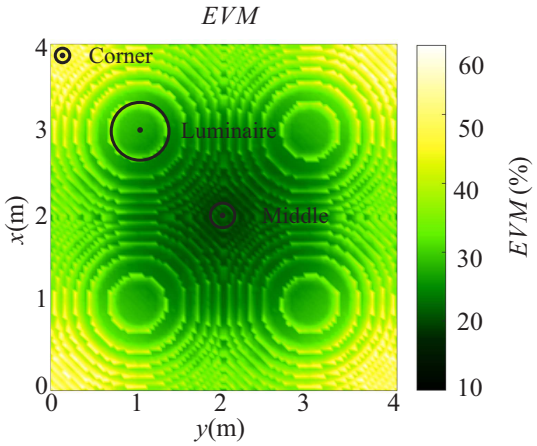

(a) Receiver positions under consideration

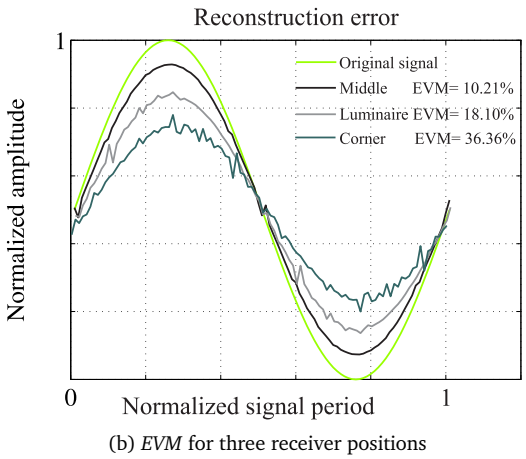

(b) *EVM* for three receiver positions

Figure 2.14: *EVM*, $f = 100$MHz, *HPA*45°, *FOV*60°

3 ODAC FRONT-ENDS DESIGN AND PERFORMANCE EVALUATION

This chapter is dedicated to the ODAC transmitter hardware design and its experimental performance testing. Specifically, two ODAC samples proposed in previous simulations are considered where the first transmitter employs white LEDs in a compact PLCC6 package while the second sample uses square-shaped 7.62mm blue LEDs.

3.1 VLC ODAC emitter

Unlike a conventional VLC emitter, where performance is affected by the LEDs inherent nonlinearity, the ODAC-based transmitter offers better linearity and no need of EDAC in the driver stage. Furthermore, the recent trends in general lighting seems to be in line with the ODAC concept in terms of multiple LED array designs or the use of COB LEDs for higher luminous output. On the other hand, the ODAC concept may suffer from a significant quantization error for small resolutions (arising from the ODAC bit depth, i.e. the total number of LED groups in the ODAC emitter array), lower modulation bandwidth, and geometrical distortion.

Figure 3.1 depicts the hardware implementation of both proposed ODAC front-ends for VLC applications. Specifically, the first ODAC front-end (figure 3.1a) employs off-the-shelf white LEDs in a PLCC6 housing. The second ODAC front-end uses conventional discrete blue LEDs encapsulated in a 7.62mm square package as depicted in figure 3.1b. The front-ends are made of double layered FR4 printed circuit board (PCB), where the top layer is dedicated to the LEDs and the bottom layer to the driving circuits.

As both front-ends have 8-bit depth, the overall LED number inside each emitter array is 255 which corresponds to $2^k - 1$. In the array, the LSB is represented by one LED, while the most significant bit (MSB) is formed by 128 LEDs. The second ODAC emitter (see figure 3.1b) is formed by 255 LED packages having an active area 122mm x 122mm.

The PLCC6 ODAC front-end(figure 3.1a) comprises of 93 PLCC6 LED packages, each containing three LED chips. Thanks to the PLCC6 surface mount technology, the circular active area dimensions of the second front-end are reduced to 60mm x 60mm. This supports a better uniformity of the optical intensity displacement in the near field radiation area.

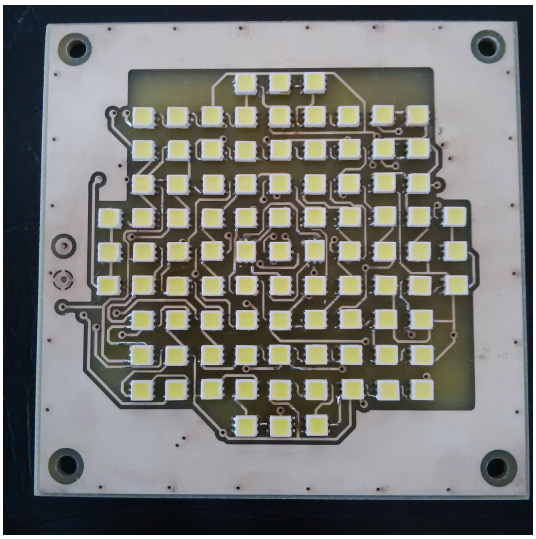

(a) PLCC6 white LED ODAC front-end

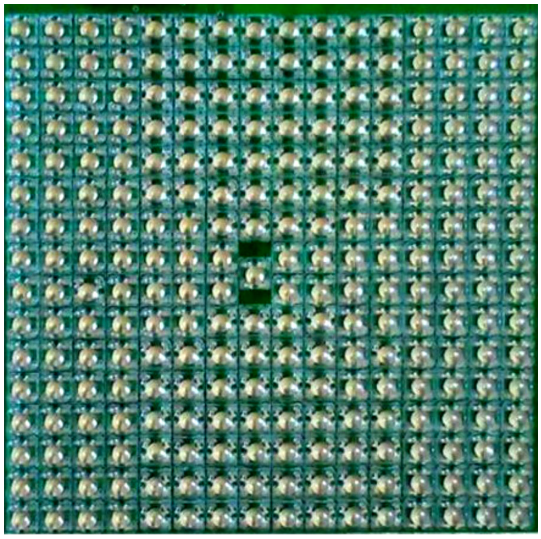

(b) 7.62mm square blue LED ODAC front-end

Figure 3.1: ODAC hardware samples

3.2 Signal reconstruction error performance

This section explores ODAC performance in terms of signal reconstruction error considering dynamic reconstruction tests.

3.2.1 Dynamic signal reconstruction tests

Figure 3.2 depicts a conceptual diagram of the experimental set-up. The evaluation board FPGA Virtex6 ML605 was programmed to generate a signal $v(t)$ which was represented by a set of bit streams $B(t)$, all having the same amplitude. These digital bit streams drove k independent LED groups in an ODAC emitter array. The transmitted bit streams were merged on the optical channel. Both ODAC front-ends under consideration employed a binary weighted approach as can be seen in figure 3.2. The optical signal impinged the optical receiver where the recovered signal $\bar{v}(t)$ was a reconstructed clone of original signal $v(t)$.

Reconstruction error E_{RMS} depended on optical channel impairments, ODAC quantization error, and ODAC distortion error induced by the geometrical set-up between the ODAC front-end and the optical receiver. The receiver side used PIN photo-diode FDS100 followed by an operational amplifier (OPA657) in gain variable transimpedance stage. The recovered signal $\bar{v}(t)$ was captured by a scope (Tektronix TDS2000C) and data was imported to MATLAB for further offline signal processing. Since the channel impulse response (CIR) of each LED in the array is given by $h(t)$ the recovered signal $\bar{v}(t)$ at the experimental chain end can be expressed by equation (3.1):

$$\bar{v}(t) = \left[R_{\mathrm{PD}} \sum_{\mathrm{m}=1}^{\mathrm{k}} \sum_{\mathrm{n}=1}^{2^{\mathrm{m}}-1} B_{\mathrm{m}}(t) * h_{\mathrm{m,n}}(t) P_{\mathrm{Tx,m,n}} \right] + n_0. \tag{3.1}$$

Performance evaluation is based on periodic signals to facilitate comparison between the original and the reconstructed signal version. In this case, a ramp-shaped signal having frequencies 1kHz and 98kHz was used. The normalized versions of $v(t)$ generated on the transmitter side and $\bar{v}(t)$ captured on the receiver side were considered.

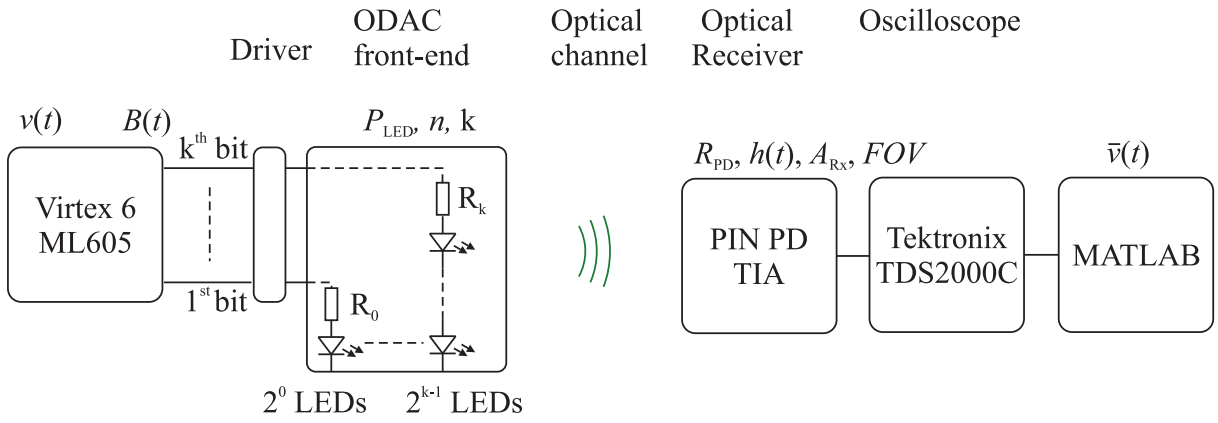

Figure 3.2: Dynamic tests set-up

Figure 3.3 illustrates reconstruction error of both ODAC samples. Specifically, in figure 3.3a and figure 3.3b the comparison between normalized versions of the reconstructed signal $\bar{v}(t)$ (green and gray curves) and the original signal $v(t)$ (black curve) is shown. Gray-colored curves in figure 3.3a illustrate huge E_{RMS} for the ODAC emitter employing discrete blue LEDs placed at a distance of 0.05m. This excessive error, in percentages 29.33% and 27.77% for frequencies 1kHz and 98kHz, respectively, was caused by the emitter's higher array dimensions inducing distortion in the emitter near field.

In the case of the PLCC6 ODAC emitter, the green-colored curves show typical values of E_{RMS}. Particularly, the E_{RMS} was 4.06% for signal frequency 1kHz and 4.01% for signal frequency 98kHz. As can be seen in figure 3.3b for a distance of 0.5m, the blue LED ODAC emitter does not suffer from excessive E_{RMS} anymore. This fact is confirmed in figure 3.3c showing E_{RMS} dependence on the distance between emitter and optical receiver. As an acceptable E_{RMS} limit, $E_{\mathrm{RMS}} = 5\%$ was considered. In the case of the blue LED front-end, this limit lies around a distance of 0.4m. Naturally, E_{RMS} increases depending on signal frequency. It is obvious in the case of the PLCC6 ODAC front-end where the slow yellowish component limited the bandwidth. The E_{RMS} for the 1kHz and 98kHz ramp signal was 0.90% and 4.81%, respectively, as illustrates figure 3.3b. Furthermore, an angular E_{RMS} measured at distance 0.5m for both ODAC samples is shown in figure 3.3d. The PLCC6 ODAC emitter exhibits better uniformity than the blue ODAC emitter regarding the error curve shape. This is a consequence of larger blue ODAC front-end active area dimensions resulting in worse optical intensity uniformity displacement in the near field radiation area [10].

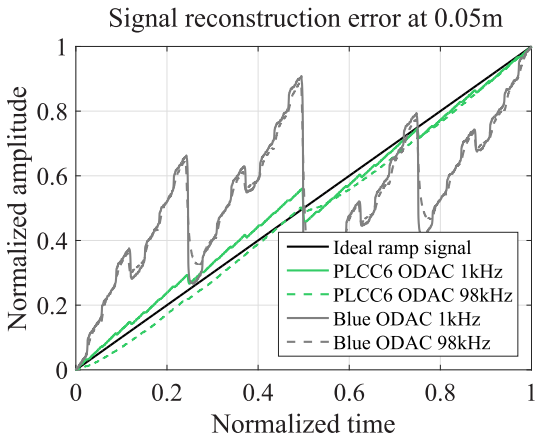

(a) Signal reconstruction error E_{RMS} at 0.05m

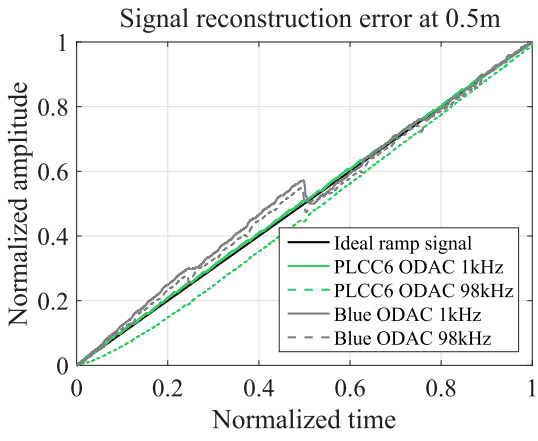

(b) Signal reconstruction error E_{RMS} at 0.05m

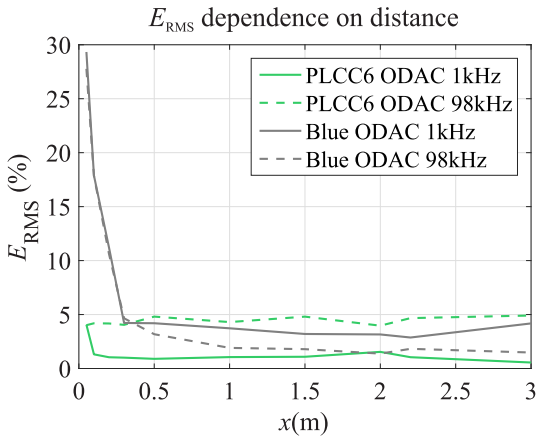

(c) E_{RMS}dependent on distance x

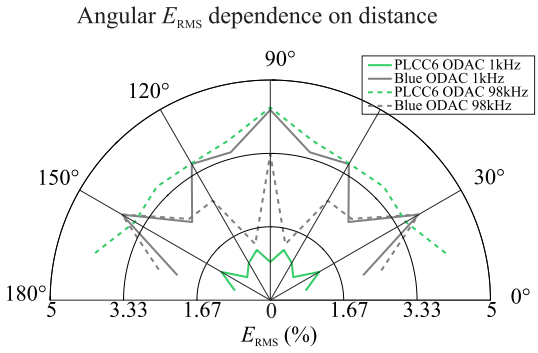

(d) Angular E_{RMS}dependence

Figure 3.3: Dynamic signal reconstruction error

3.3 Linearity error performance

From the perspective of transfer function linearity, a conventional EDAC can be specified by integral non-linearity (INL) and differential non-linearity (DNL). Similarly, the same approach can be applied for ODAC specification. Integral non-linearity is defined as the maximum deviation at any point in the transfer function from an ideal characteristic which can be expressed by equation (3.2) [10]:

$$INL(t) = \frac{V_{\text{Out}}(t) - V_{\text{Ideal}}(t)}{V_{\text{LSB}}}, \tag{3.2}$$

where $V_{\text{Out}}(t)$ is voltage amplitude measured at the output of the optical receiver, $V_{\text{Ideal}}(t)$ is the ideal receiver voltage output amplitude, V_{LSB} denotes the voltage corresponding to 1LSB and t corresponds to the discrete time of input signal $v(t)$ sample [10].

Differential nonlinearity $DNL(t)$ describes the maximum deviation of the actual and ideal (+1LSB) analog output step between two adjacent input codes as denotes equation (3.3). Moreover, when $DNL(t)$ exceeds -1LSB the DAC transfer function is non-monotonic [20].

$$DNL(t) = \frac{V_{\text{Out}}(t+1) - V_{\text{Ideal}}(t)}{V_{\text{LSB}}} - 1. \tag{3.3}$$

Unlike in EDAC, the linearity error in ODAC also depends on the geometrical set-up between the ODAC emitter and the optical receiver. In order to demonstrate how ODAC $INL(t)$ and $DNL(t)$ depend on geometrical considerations, the following graphs in figures 3.4 and 3.5 include additional information on distance between the emitter and optical receiver. Figure 3.4 graphically represents $INL(t)$ and $DNL(t)$ of the 7.62mm square LED blue ODAC emitter. Apparently, $INL(t)$ dominates for signal frequency of 95kHz. Needless to say, the highest $INL(t)$ is spread in front of the emitter due to the optical intensity non-uniformity as was described formerly. As illustrates figure 3.5, $INL(t)$ and $DNL(t)$ increase at higher frequencies (98kHz) is a result of PLCC6 LED bandwidth shortage [10].

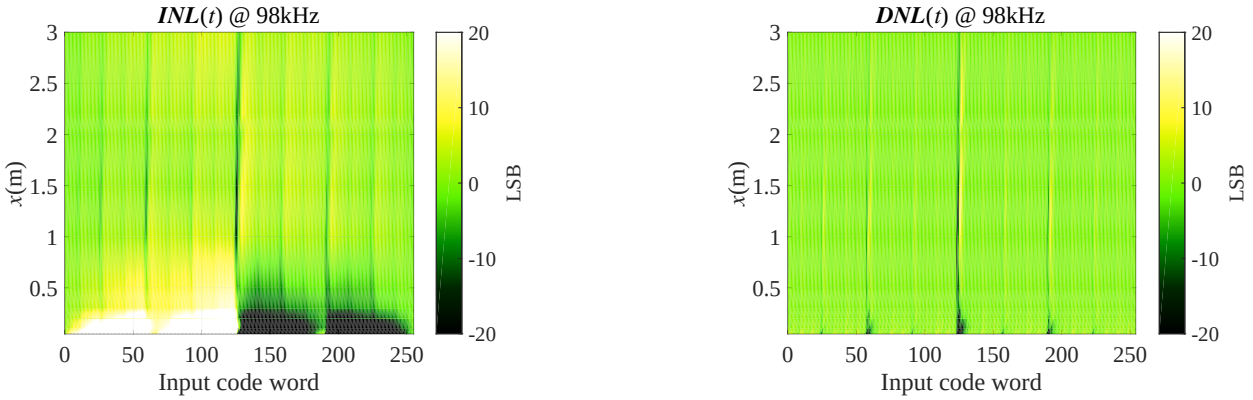

(a) $INL(t)$ (b) $DNL(t)$

Figure 3.4: Blue 7.62mm LED ODAC front-end, $f = 98kHz$

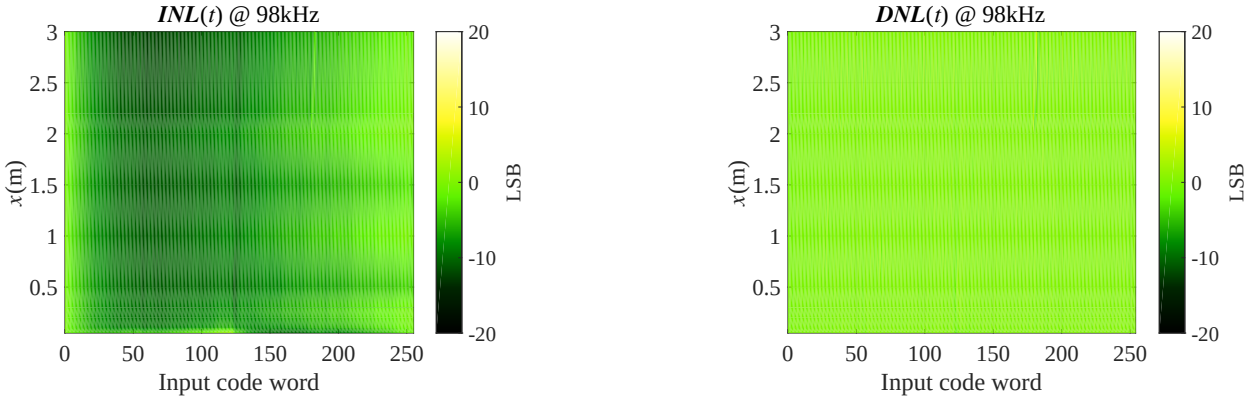

(a) $INL(t)$ (b) $DNL(t)$

Figure 3.5: Blue 7.62mm LED ODAC front-end, $f = 98kHz$

3.4 Real time FPGA-based VLC system

Figure 3.6 shows experimental test bed diagram of the real-time FPGA-based VLC system.

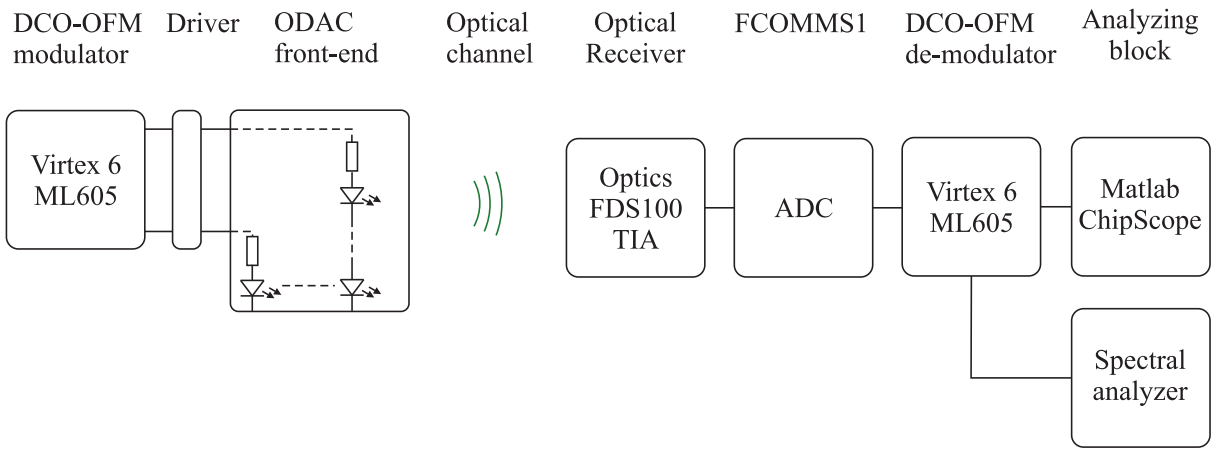

Figure 3.6: Real time FPGA-based OFDM VLC system set-up diagram

The transceiver was able to generate DCO-OFDM signals with configurable bandwidth, allowing to evaluate performance for increasing data rates. The digital component of the communication system was implemented in a Xilinx Virtex-6 FPGA, while the AD conversion on the receiver side was implemented in an Analog Devices FMCOMMS1 board, in a similar manner as described in [17] and used in [11].

Figure 3.7 shows *BER* results for increasing distances and transmitted data-rates. The figure also shows the forward error correction (FEC) limit boundary $3.8 \cdot 10^{-3}$. At shorter distances (less than 60cm), the receiver gain had to be reduced to avoid overcoming the ADC dynamic range which would result in signal clipping. The VLC system performance degraded with distance but still achieved over 19Mbps for distances compatible with the typical scenario where the luminaire is on the ceiling and the receiving devices are on a table top ($\approx$ 2.2m). The maximum measured data rate was 30Mbps at 1m. Below 80cm, *BER* performance started getting affected by the ODAC emitter geometric distortion and receiver saturation in this arrangement due to the lens in the receiver, LEDs with high *HPA* and a PD with wide *FOV*. Using the same setup, distances and data-rates (figure 3.8), the received constellation's *EVM* was measured in order to infer the relationship between *BER* and *SNR* [12].

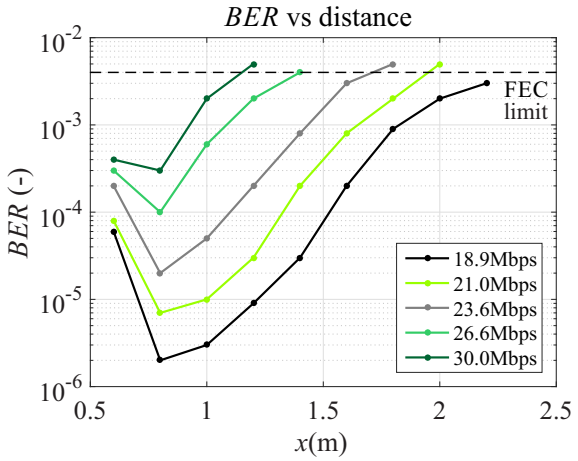

Figure 3.7: *BER* performance for increasing distances and bitrates

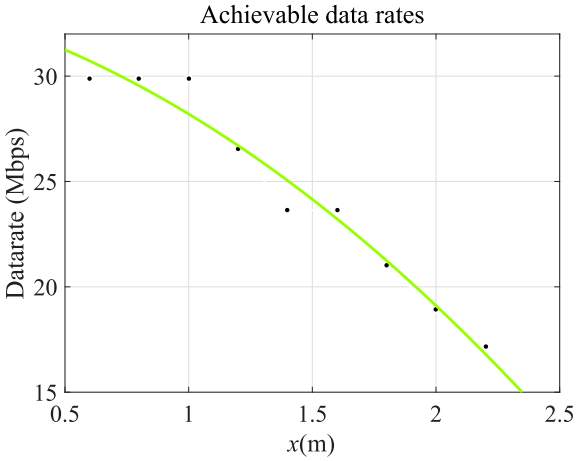

Figure 3.8: Achievable datarates for distances from 60cm to 220cm

4 CONCLUSION

The doctoral thesis is focused on utilizing the optical D/A converter concept in optical wireless communication systems working in the area of visible light. Initially, the thesis outlines the essential introduction into VLC systems. The thesis summarizes possible types of VLC transmitters, describes particular types of receivers and presents an overview of modulations which may be utilized in VLC. In addition, the first chapter presents available channel modeling techniques suitable to characterize optical channel impairments in VLC systems.

The crucial part of the thesis is focused on optical channel modeling of the communication system employing the ODAC emitter as an appropriate alternative to the conventional VLC transmitter front-end. The proposed ODAC concept seems to be an ideal candidate to outperform the conventional approach of the transmitter front-end implementation in VLC systems. Provided an ODAC-based front-end is used, there is no need for an EDAC in the transmitter stage. Inherent LED nonlinearity

is mitigated using this ODAC concept. Moreover, the ODAC concept architecture is in line with the recent trend of general lighting with respect to using multiple LED arrays.

The thesis looks into the influence of the ODAC emitter bit depth, emitter LED array topology, and the communication system geometrical arrangement as a paramount factor for the received signal quality. Furthermore, the thesis, for the first time, includes complex channel impulse response modeling of an ODAC-based VLC system, important for high data rate applications, including the first and second reflection contribution.

In the simulation part, the thesis explored several types of ODAC emitters having different topologies and dimensions. The greatest benefit of the work lies in a numerical model implemented in MATLAB able to model an optical channel of VLC systems employing the ODAC emitter on the transmitter side. The proposed channel modeling uses a deterministic ray model from the perspective of energy distribution over the channel. The thesis describes three different VLC system scenarios, in detail, with one reflection contribution ideal for slow data rates, the scenario assumes an ITS VLC system and an indoor VLC system comprising of four ODAC emitter arrays in an empty room.

In the experimental part, two ODAC functional samples were designed and implemented based on previous findings. In order to complete the VLC system for following performance evaluating, a wide-band optical receiver was developed particularly for this experimental part as well.

The ODAC-based VLC system performance is examined based on several tests. Specifically, static and dynamic signal reconstruction tests showed the ODAC emitter error performance in terms of geometrical and input signal frequency dependence. The results match expected simulation results and demonstrate typical increased signal distortion in front of the ODAC emitter. Furthermore, channel impulse response and frequency response for both ODAC samples were explored. In order to investigate nonlinear error performance, the experimental part includes INL and DNL tests tailored especially for the ODAC-based VLC system. In other words, the tests included spatial dependence of both errors. Finally, the thesis presents, for the first time, real time an FPGA-based VLC system employing the ODAC emitter in the transmitter stage. VLC high data rate communication was demonstrated despite the ODAC emitter limited bandwidth.

BIBLIOGRAPHY

[1] Traffic light signals. Technical and functional requirements. Part 1: Traffic light signals for traffic control. Printed, 1997.

[2] Traffic light signals. Location and use of signal heads. Printed, March 1994.

[3] Design of urban roads. Printed, January 2006.

[4] BARRY, J. R. et al. Simulation of Multipath Impulse Response for Indoor Wireless Optical Channels. *IEEE Journal on selected areas in communications*. April 1993, 11, 3, s. 367–379.

[5] CREE. Cree First to Break 300 Lumens-Per-Watt Barrier. Technical report, Cree, Inc., 2014.

[6] DOBESCH, A. – ALVES, L. N. – WILFERT, O. On the Performance of Digital to Analog Conversion in the Optical Domain for Low Data Rate Communications. In *Transparent Optical Networks (ICTON), 2014 16th International Conference*, s. 1–4, August 2014. doi: 10.1109/ICTON.2014.6876676.

[7] DOBESCH, A. – ALVES, L. N. – WILFERT, O. Spatial ODAC performance for indoor environment. In *Optical Wireless Communications (IWOW), 2014 3rd International Workshop*, s. 1–5, September 2014. doi: 10.1109/IWOW.2014.6950779.

[8] DOBESCH, A. et al. ODAC-based traffic lights for intelligent transport systems. In *26th Conference Radioelektronika 2016*, s. 1–5. IEEE, May 2016. doi: 10.1109/RADIOELEK.2016.7477401.

[9] DOBESCH, A. et al. Optical Digital to Analog Conversion Performance Analysis for Indoor Set-up Conditions. *Optics Communications*. May 2017, 400, s. 115–122. doi: 10.1016/j.optcom.2017.05.021.

[10] DOBESCH, A. et al. Performance analysis of 8-bit ODACs for VLC applications. *Radioen*. June 2017, 26, 2, s. 418–422. doi: 10.13164/re.2017.0418.

[11] FIGUEIREDO, M. – ALVES, C. R. L. N. Live demonstration: 150Mbps+ DCO-OFDM VLC. In *Circuits and Systems (ISCAS)*, s. 457. IEEE, August 2016. doi: 10.1109/ISCAS.2016.7527275.

[12] FIGUEIREDO, M. et al. Consumer LED lamp with ODAC technology for high-speed Visible Light Communications. *IEEE Transactions on Consumer Electronics*. Accepted for publication.

[13] HAAS, H. et al. What is LiFi? *Journal of Lightwave Technology*. March 2015, 34, 6, s. 1–12. doi: 0.1109/JLT.2015.2510021.

[14] HEROLD, M. – ROBERTS, D. Spectral characteristics of asphalt road aging and deterioration: implications for remote-sensing applications. *Applied Optics*. 2005, 44, 20, s. 4327–4334.

[15] KAHN, J. M. – BARRY, J. R. Wireless infrared communications. *Proceedings of the IEEE*. 1997, 85, s. 265–298.

[16] MORGAN, F. Gauging the lifetime of an LED. Technical report, Digital Lumens, 2012.

[17] RIBEIRO, C. – FIGUEIREDO, M. – ALVES, L. N. A Real-Time Platform for Collaborative Research on Visible Light Communication. In *Optical Wireless Communications (IWOW)*, s. 112–116. IEEE, 2015. doi: 10.1109/IWOW.2015.7342277.

[18] TANAKA, Y. – HARUYAMA, S. – NAKAGAWA, M. Wireless optical transmissions with white colored LED for wireless home links. In *Personal, Indoor and Mobile Radio Communications*, 2, s. 1325–1329, 2000. doi: 10.1109/PIMRC.2000.881634.

[19] UEMOTO, K. L. – SATO, N. M. N. – JOHN, V. M. Energy and Buidlings. *International Conference on Building Energy and Enviroment*. 2010, 42, s. 17/22.

[20] BOSCH, A. – STEYAERT, M. – SANSEN, W. *Static and Dynamic Performance Limitations for High Speed D/A Converters*. Springer Science & Business Media, 2004.

Ales Dobesch

16.3.1989
00420 541 14 6558
xdobes05@stud.feec.vutbr.cz

Research interests

Visible light communication with special emphasis on optical channel modeling, transmitter and receiver hardware design. Free space optical communication with focus on hardware design and implementation.

Education

Since 09/2013 Brno University of Technology, Brno, Czech Republic

- Doctor of Philosophy (Ph.D.), Electronics and Communication
- An optical D/A converter for VLC applications

09/2011 - 06/2013 Brno University of Technology, Brno, Czech Republic

- Master's degree (Ing.), Electronics and Communication
- IR Thermometer with Automatic Emissivity Correction
- Dean's award

09/2008 - 06/2011 Brno University of Technology, Brno, Czech Republic

- Bachelor's (Bc.) degree: Radioelectronics
- Design and Realization of D Class Audio Amplifier Controlled by Microcontroller
- Dean's award

Academic appointments

Since 09/2013 Department of Radioelectronics, Brno University of Technology

Since 09/2013 Sensor, Information and Communications Systems (SIX) research group

Research stays

1/2014 - 2/2014 Short Time Scientific Mission within COST IC1101 project University of Aveiro, Portugal.

- Optical channel modeling of the ODAC concept
- Supervised by: Prof. Luis Nero Alves

11/2015 - 12/2015 Internship within University of Leiria, Portugal.

- Real time FPGA-based VLC communication system
- Supervised by: Prof. Luis Nero Alves, Prof. Carlos Gaspar Ribeiro, Monica de Figueiredo

Computer skills

- Matlab, Simulink, C/C++, VHDL
- Microsoft office, LYX, LaTex
- CorelDraw Suite, Adobe Photoshop
- AutoCAD, PSPICE, Eagle CADsoft
- Labview, AVR Studio, VEE Agilent

Languages

- Czech - Native speaker
- English - Upper intermediate
- German - Intermediate

ABSTRACT

The dissertation deals with the optical digital to analog converter as an alternative transmitter front-end concept for visible light communication applications. The dissertation looks into optical channel modeling and suggests a suitable modeling approach. A significant part devoted to the numerical optical channel modeling reveals the influence of emitter bit depth, emitter array topology and geometrical arrangement on communication system performance. The dissertation deals with optical digital to analog converter design based on previously acquired simulations and explores overall front-end performance. Furthermore, the thesis presents a real time demonstration of high data rate optical communication using the front-end.

ABSTRAKT

Disertační práce se zabývá optickým digitálně-analogovým převodníkem, jako alternativou optické části koncové vysílací jednotky (optický front-end) určené pro VLC (visible light communication) aplikace. Stěžejní část práce, která se věnuje numerickému modelování optického kanálu, prezentuje vliv bitové hloubky, topologie koncové části optického vysílače a geometrického uspořádání na přenášený signál. Součástí práce je návrh, realizace a ověření parametrů optického digitálně-analogového převodníku vycházející z předcházejících simulací. V poslední řadě práce obsahuje demonstraci vysokorychlostní optické komunikace s využitím navrženého VLC optického vysílače.

DOBESCH, A. An optical D/A converter for VLC applications. Brno: Brno University of Technology, Faculty of Electrical Engineering and Communication, 2017. 37 p. Supervised by Prof. Ing. Otakar Wilfert, CSc.